Journal of Zhejiang University-SCIENCE A (Applied Physics & Engineering) in press
www.jzus.zju.edu.cn; www.springer.com/journal/11582
E-mail: jzus_a@zju.edu.cn

Research Article

https://doi.org/10.1631/jzus.A2400194

Multi-scale analysis of the self-vibration of a liquid crystal elastomer fiber-spring system exposed to constant-gradient light

Haiyang WU, Jiangfeng LOU, Yuntong DAI, Biao ZHANG, Kai LI✉

School of Civil Engineering, Anhui Jianzhu University, Hefei 230601, China

Abstract: Self-vibrating systems comprised of active materials have great potential for application in the fields of energy harvesting, actuation, bionic instrumentation, and autonomous robotics. However, it is challenging to obtain analytical solutions describing these systems, which hinders analysis and design. In this work, we propose a self-vibrating liquid crystal elastomer (LCE) fiber-spring system exposed to spatially-constant gradient light, and determine analytical solutions for its amplitude and period. First, using a dynamic model of LCE, we obtain the equations governing the self-vibration. Then, we analyze two different motion states and elucidate the mechanism of self-vibration. Subsequently, we derive analytical solutions for the amplitude and frequency using the multi-scale method, and compare the solutions with numerical results. The analytical outcomes are shown to be consistent with the numerical calculations, while taking far less computational time. Our findings reveal the utility of the multi-scale method in describing self-vibration, which may contribute to more efficient and accurate analyses of self-vibrating systems.

Key words: Self-vibration; Constant-gradient light; Liquid crystal elastomer; Multi-scale method

1 Introduction

Self-sustained motions are movements which harvest energy from stable ambient motion to sustain themselves (Li et al., 2013; Wang et al., 2018; Nocentini et al., 2018; Ge et al., 2018). Self-vibrations are a prominent example, and have recently garnered significant research attention (Preston et al., 2019; Zeng et al., 2019; Ding, 2010). As opposed to forced oscillations, self-vibrations can maintain continuous oscillation without the need for external control or energy input. This property makes self-vibrating systems extremely useful for micro-controller applications (Baumann et al., 2018; Kageyama et al., 2020; Liao et al., 2019; White et al., 2008). Self-vibration is a characteristic nonlinear dynamic process (Fang et al., 2019), and its study can lead to a deeper understanding of synchronization (Thomson, 2005; Pivnenko et al., 1999; Wu et al., 2024), chaotic, and bifurcation (Xu et al., 2024; Kumar et al., 2016; Xu et al., 2024) behavior in nonlinear systems. Moreover, it finds application in diverse areas such as autonomous separators (Shastri et al., 2015), soft robotics (He et al., 2023; Wang et al., 2023), motors (Yu et al., 2024)., and bionic devices (Sun et al., 2021).

Recently-developed self-vibrating systems have been constructed from a range of materials, including ionic gels (Boissonade and Kepper, 2011; Hua et al., 2021), hydrogels (Yoshida, 2010), polymers (Wang et al.,2022; Wang et al., 2021; Chen et al., 2021; Hu et al., 2021), and liquid crystal elastomers (LCEs) (Wang et al., 2023; Dai et al., 2023; Yang et al., 2023; Chen et al., 2024; Bai et al., 2024; Wang et al., 2020). When exposed to light (Kumar et al., 2016), heat (Guo et al., 2022; Cui et al., 2019), electricity (Liao et al., 2022), magnetism (Haber et al., 2013), chemical reactions (Wang et al., 2022; Harris et al., 2005), or other external stimuli, these systems can change shape or display different kinematic modes. Considering the various reactions of different materials to external stimuli, self-vibrating systems such as oscillating (Wu et al., 2024; Wu et al., 2023; Liu et al.,

✉ Kai LI, kli@ahjzu.edu.cn
Kai Li, https://orcid.org/0000-0003-4898-2827

Received Apr. 16, 2024; Revision accepted July 1, 2024; Crosschecked

© Zhejiang University Press 2024

Unedited

2024; Zuo et al., 2023), chaotic (Xu et al., 2024), rotating (Yu et al., 2024), buckling (Ge et al., 2023), bending (Manna et al., 2021; Li et al., 2021), rolling (Bazir et al., 2020), vibrating (Zhou et al., 2024), shuttling (Yu et al., 2022), jumping (Kim et al., 2021), galloping (Yu et al., 2024), floating (Cheng et al., 2023), and swimming (Serak et al., 2010) forms have been proposed. Moreover, self-oscillators originating from distinct feedback mechanisms have seen extensive development; some of these mechanisms include the coupling of liquid volatilization with membrane deformation (Chakrabarti et al., 2020), the coupling of large deformations with chemical reactions (Boissonade et al., 2011) the coupling of multiple processes involving water absorption/desorption with film bending (Fu et al., 2022), as well as self-shading mechanisms (Bazir et al., 2020; Cheng et al., 2019). Such diverse self-vibrating systems can be applied to develop actuators and micro-controllers, harvest energy, and perform other functions.

At present, the primary research focus on self-oscillating systems is understanding their characteristics, such as amplitude, frequency, and equilibrium position (Xu et al., 2024; Wu et al., 2023). To obtain such properties, computational software is often used to numerically simulate the governing equations, allowing determination of time-history curves and phase diagrams. These numerical results allow analysis of the motion regimes of self-oscillating systems, as well as estimation of their characteristic amplitude and frequency. Understanding these properties aids the design of other self-oscillators and informs motion regulation strategies. Research has shown how system parameter adjustment can regulate the behavior of self-oscillators; for example, the damping factor can suppress the amplitude and enhance the period (Wu et al., 2024; Kim et al., 2021), while the elastic factor can enhance the amplitude and suppress the period. In addition, for LCE-based self-vibrating systems, their amplitude and frequency rise when the light intensity and contraction factor are increased (Yu et al., 2024). Changing certain system parameters can even give rise to new self-vibrating properties, such as synchronization (Thomson, 2005; Pivnenko et al., 1999; Wu et al., 2024) and chaos (Xu et al., 2024; Kumar et al., 2016; Xu et al., 2024).

Various numerical methods have been applied to self-oscillating systems, including the Runge-Kutta (McLachlan et al., 2011), shooting and multi-shooting (März, 1984), finite difference (Patidar et al., 2005), and continuation methods (Allgower and Georg, 2012). Among these the Runge-Kutta method is currently the most popular, but it has limitations such as high computational complexity and difficult programming implementation. In order to solve nonlinear systems such as self-oscillators, many analytical or semi-analytical methods have been explored, including the average method, multi-scale method (Fan and Shen, 2022; Li, et al., 2004; Min et al., 2020; Wen, et al., 2007), asymptotic method (Panton, 2013), and others (Cheung et al., 1990; Yan et al., 2023; Vestroni et al., 2008). From these, the multi-scale method has been most widely used due to its high efficiency and accuracy. The multi-scale method is a mathematical approach first proposed by Ali H. Nayfeh (Nayfeh, 1965), which he has since used for applications in mass spectrometry, perturbed nonlinear systems (Nayfeh and Mook, 1979; Nayfeh, 1993), and astronomy (Nayfeh and Pai, 2008). In addition, Sturrock applied the perturbation method to dynamically analyze electron plasma (Sturrock PA and surName, 1957).

He et al. have recently reported the occurrence of self-vibrations in LCE microfibers in a steady temperature field (He et al., 2021). In their experimental setup, LCE microfibers were suspended from a rigid plate. These microfibers experienced an irregular yet constant temperature field, created by a heat source at the base. Within a short time, the attached mass block demonstrates continuous vibration, as shown in Fig. 1. To analyze the self-vibrational properties of analogous LCE fiber-mass systems, we first construct a model of an LCE fiber-spring system. Analytical solutions are then derived for the amplitude and frequency of the self-vibration. Our goal is to improve the understanding of LCE fiber-spring systems and provide a useful reference for those developing new self-vibrating systems using active materials.

This study is organized as follows. Section 2 introduces a theoretical model for the self-oscillator exposed to spatially-constant gradient light. Section 3 explores two distinct motion regimes identified through numerical calculation, which elucidate the mechanism of self-vibration. Then in Section 4, we perform bifurcation analysis using the Hurwitz crite-

Unedited

rion (Heller, 2005; Ho et al., 1998), and determine the amplitude and period using the multi-scale method. The impact of system conditions is then investigated. Finally, Section 5 summarizes the key findings.

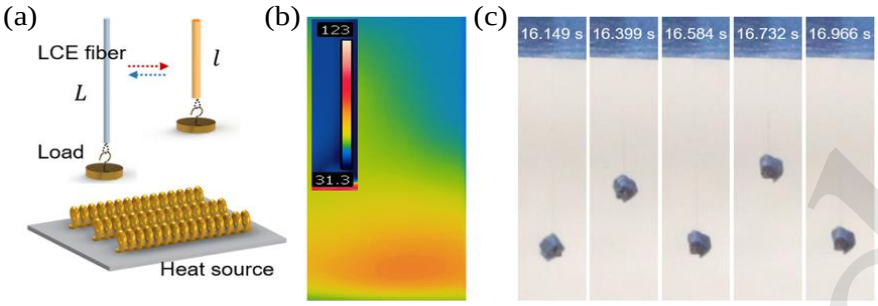

Fig. 1. Self-vibration of an LCE microfiber on a heated platform. (a) An LCE fiber on a heat source. (b) The temperature distribution. (c) Sequential images showcasing the continuous oscillation of the mass block under steady thermal conditions (He et al., 2021)

2 Theoretical model and formulation

Here, we present an LCE fiber-spring self-oscillator exposed to spatially-constant gradient light. Utilizing a dynamic LCE model, we derive the governing equations for the system. Finally, we non-dimensionalize the governing equations and introduce the solution method.

2.1 Dynamics of the LCE fiber-spring system

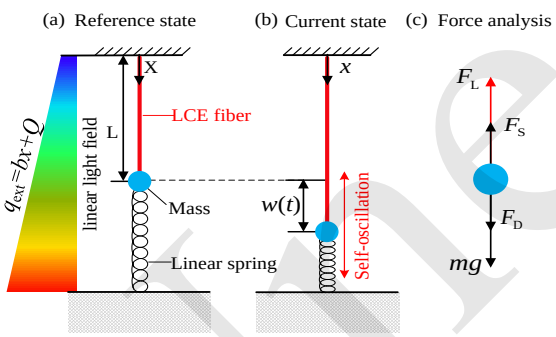

Fig. 2. The system exposed to spatially-constant gradient light: (a) Reference state, (b) Current state, and (c) Force analysis.

Fig. 2 shows a model diagram of the system, which is comprised of an LCE fiber, a linear spring, and a mass block. Fig. 2(a) shows the LCE fiber-spring system in its reference state, where the LCE fiber and the linear spring are at their original lengths. A spatially-constant gradient light is shone on the LCE fiber. This illumination heats the LCE fiber, causing it to undergo contraction in the vertical direction. The initial deformation alters the light distribution across the LCE fiber, thereby facilitating greater deformation of the fiber. Gravity also stretches the fiber, and the spring and the LCE fiber produce restoring forces in response. Under this combination of factors, self-vibration may occur. Fig. 2(b) shows the displacement $w(t)$ of the LCE fiber's end in the vertical direction. Fig. 2(c) illustrates the force analysis of the mass block. Here, F_L denotes the tension of the LCE fiber, F_S represents the elastic force of the spring, F_D signifies the damping force, and mg is the gravitational force, where m is the mass and g is the gravitational acceleration. Here, we derive the dynamic governing equation of the system:

$$m\ddot{w}(t)=mg+F_L+F_D+F_S, \qquad (1)$$

where $\ddot{w}(t)$ denotes the acceleration.

The elastic force of the spring and the displacement of the LCE fiber end comply with Hooke's law, and is calculated as:

$$F_S(w)=K_S w(t) \qquad (2)$$

where $w(t)$ is the end displacement of the LCE fiber, and K_S is the elastic factor of the spring.

2.2 Dynamics of the LCE fiber-spring system

For ease of derivation and explanation, a Lagrangian coordinate system X and a Eulerian coordinate system x are established for the reference state and current state, respectively. This is depicted in Fig. 2. The instantaneous position and displacement of a particle in the LCE fiber are denoted as $x(t)$ and $u(t)$, respectively. The relationship between $x(t)$ and $u(t)$ is $x(t)=u(t)+X$.

We hypothesize that elastic force is proportional to the amount of elongation, and can be written as:

$$F_L=K_L L[\varepsilon(X,t)-\varepsilon_T(X,t)] \qquad (3)$$

where K_L and L are the elastic factor and original

Unedited

length of the fiber, respectively, $\varepsilon(X,t)$ indicates the total strain, and $\varepsilon_{\mathrm{T}}(X,t)$ denotes the photothermally-driven strain. The total strain can be expressed as:

$$\varepsilon(X,t)=\frac{\partial u(X,t)}{\partial X} \tag{4}$$

The photothermally-driven strain of LCE fiber with temperature is generally nonlinear. Here, it is assumed that the deformation is small, and the change of photothermally-driven strain with temperature is approximately linear, i.e.:

$$\varepsilon_{\mathrm{T}}(X,t)=CT(X,t) \tag{5}$$

where C denotes the thermal contraction factor of LCE, and $T(X,t)$ indicates the temperature of the LCE fiber at $x=X$.

For simplicity, we assume a uniform distribution of tension across the LCE fiber, being equal everywhere. Consequently, the fiber tension at $X=L$ can be expressed as:

$$F_{\mathrm{L}}(t)=K_{\mathrm{L}}\left[w(t)-C\int_0^L T(X,t)dX\right] \tag{6}$$

For simplification, we assume uniform heating across a given cross section. The system constantly exchanges heat with the external environment, and the temperature therefore satisfies:

$$\rho_{\mathrm{C}}\frac{\mathrm{d}T(X,t)}{\mathrm{d}t}=q_{\mathrm{ext}}(x)-K_{\mathrm{H}}T(X,t) \tag{7}$$

where ρ_{C} represents the specific heat capacity, K_{H} denotes the heat transfer factor, and $\tau=\frac{\rho_{\mathrm{C}}}{K_{\mathrm{H}}}$ indicates the characteristic time. The heat flux from the constant-gradient light is $q_{\mathrm{ext}}(x)=bx+Q$, where b is the gradient of the heat flux and Q is the heat flux at $x=0$.

2.3 Asymptotic analysis

We define the following dimensionless parameters: $\bar{t}=t/\sqrt{\mathrm{L/g}}$, $\bar{F}_{\mathrm{L}}=F_{\mathrm{L}}/mg$, $\bar{u}=u/L$, $\bar{w}=w/L$, $\bar{X}=X/L$, $\bar{x}=x/L$, $\bar{\tau}=\tau/\sqrt{\mathrm{L/g}}$, $\bar{K}_{\mathrm{L}}=K_{\mathrm{L}}L/mg$, $\bar{K}_{\mathrm{S}}=K_{\mathrm{S}}L/mg$, $\bar{C}=\bar{C}T_{\mathrm{L}}$, $\bar{T}=T/T_{\mathrm{L}}$, $\bar{q}_{\mathrm{ext}}=q_{\mathrm{ext}}/K_{\mathrm{H}}T_{\mathrm{L}}$, $\bar{b}=bL/T_{\mathrm{L}}$, and $\bar{Q}=Q/T_{\mathrm{L}}$ (T_{L} is the temperature at $x=L$).

Combining Eqs. (4)-(7), we can obtain the tension of the LCE fiber (Details of the derivation can be found in Section S1 of electronic supplementary materials):

$$\bar{F}_{\mathrm{L}}(\bar{t})=\frac{\bar{K}_{\mathrm{L}}\bar{C}\bar{b}}{e^{\bar{C}\bar{b}}-1}\bar{w}(\bar{t})+\bar{K}_{\mathrm{L}}\bar{C}\bar{b}\,\bar{\tau}\frac{1-e^{\bar{C}\bar{b}}+\bar{C}\bar{b}e^{\bar{C}\bar{b}}}{\left(e^{\bar{C}\bar{b}}-1\right)^2}\dot{\bar{w}}(t)+\bar{K}_{\mathrm{L}}\left(\frac{\bar{C}\bar{b}}{e^{\bar{C}\bar{b}}-1}-1-\bar{C}\bar{Q}\right) \tag{8}$$

2.4 Solution method

Inserting Eqs. (2), (3), and (8) into Eq. (1), we obtain the dimensionless form of Eq. (1) as:

$$\ddot{\bar{w}}(\bar{t})-1+\frac{\bar{K}_{\mathrm{L}}\bar{C}\bar{b}}{e^{\bar{C}\bar{b}}-1}\bar{w}(\bar{t})+\bar{K}_{\mathrm{L}}\bar{C}\bar{b}\,\bar{\tau}\frac{1-e^{\bar{C}\bar{b}}+\bar{C}\bar{b}e^{\bar{C}\bar{b}}}{\left(e^{\bar{C}\bar{b}}-1\right)^2}\dot{\bar{w}}(\bar{t})+\bar{K}_{\mathrm{S}}\bar{w}(\bar{t})+\bar{F}_{\mathrm{D}}(\bar{t})+\bar{K}_{\mathrm{L}}\left(\frac{\bar{C}\bar{b}}{e^{\bar{C}\bar{b}}-1}-1-\bar{C}\bar{Q}\right)=0 \tag{9}$$

In practical scenarios, damping typically depends on the velocity $\dot{\bar{w}}(t)$. Therefore, we conduct a Taylor series expansion and keep the second order term, obtaining the damping force as:

$$\bar{F}_{\mathrm{D}}(\dot{\bar{w}})=(\bar{\beta}_1+\bar{\beta}_2\left|\dot{\bar{w}}(t)\right|)\dot{\bar{w}}(t) \tag{10}$$

where $\bar{\beta}_1$ and $\bar{\beta}_2$ are the first and second damping factors, respectively.

Combining Eqs. (9) and (10) yields:

$$\ddot{\bar{w}}(\bar{t})-1+\frac{\bar{K}_{\mathrm{L}}\bar{C}\bar{b}}{e^{\bar{C}\bar{b}}-1}\bar{w}(\bar{t})+\bar{K}_{\mathrm{L}}\bar{C}\bar{b}\,\bar{\tau}\frac{1-e^{\bar{C}\bar{b}}+\bar{C}\bar{b}e^{\bar{C}\bar{b}}}{\left(e^{\bar{C}\bar{b}}-1\right)^2}\dot{\bar{w}}(\bar{t})+\bar{K}_{\mathrm{S}}\bar{w}(\bar{t})+(\bar{\beta}_1+\bar{\beta}_2|\dot{\bar{w}}(\bar{t})|)\dot{\bar{w}}(\bar{t})+\bar{K}_{\mathrm{L}}\left(\frac{\bar{C}\bar{b}}{e^{\bar{C}\bar{b}}-1}-1-\bar{C}\bar{Q}\right)=0 \tag{11}$$

By substituting the system parameters into Eq. (11) and solving the equation numerically, we can obtain the system's time response curve.

3 Two motion states and mechanism

First, the static and self-vibrating regimes are delineated in this section. Then, the mechanism of the self-vibration is investigated based on the dynamic properties.

3.1 Solution method

To understand the system's self-vibrational properties, it's imperative to determine the dimensionless parameters. Sourced from existing literature (Liu et al., 2024; Nagele et al., 1997), Table 1 outlines the standard values of system parameters, while Table 2 showcases dimensionless ranges of these parameters.

Unedited

Table 1. System parameters

Parameter	Definition	Value	Unit
L	Original fiber length	0.1	m
g	Gravitational acceleration	9.8	m/s^2
K_L	Elastic factor of LCE fiber	0.1~15	N/m
K_S	Elastic factor of spring	0.1~15	N/m
C	Thermal contraction factor	-0.05~-0.01	$1/^\circ C$
b	Gradient of heat flux	0~150	$^\circ C/m$
β_1	First damping factor	0.001~0.004	kg/s
β_2	Second damping factor	0~0.02	kg/s
τ	Characteristic time	0~0.2	s
m	Mass	0.01	kg

Table 2. Dimensionless range

Parameter	$\overline{K}_L$	$\overline{K}_S$	$\overline{C}$	$\overline{b}$	$\overline{\beta}_1$	$\overline{\beta}_2$	$\overline{\tau}$
Value	0~10	0~16	-0.5~-0.1	0~1.5	0~0.04	0~0.2	0~0.02

We take the first damping factor $\overline{\beta}_1$ as an example, where $\overline{K}_L = 10$, $\overline{K}_S = 5$, $\overline{C} = -0.3$, $\overline{b} = 1$, $\overline{\beta}_2 = 0.05$, $\overline{\tau} = 0.01$. With $\overline{\beta}_1 = 0.05$, the system amplitude decays until it reaches zero as shown in Figs. 3(a) and (b); i.e. the system is in the static regime. With $\overline{\beta}_1 = 0.01$, the system is in a self-vibration regime as depicted in Figs. 3(c) and (d). Similar to existing experimental results (He et al., 2021), the LCE fiber-spring system has two regimes: the static regime and self-oscillation regime. Notably, the total strain of the LCE fiber is less than 10% during the simulation, which agrees with existing experiments (He et al., 2021). This is because the LCE fiber absorbs heat energy from the constant-gradient light, and gains kinetic energy to compensate for the damping dissipation. When the first damping factor is 0.05 or greater, the damping dissipation prevails, and the energy acquired by the LCE fiber cannot offset this dissipation. Consequently, the system's motion eventually halts, entering a static regime. This behavior is illustrated in Fig. 3(b) where the phase trajectory converges to a singular point. Conversely, when the first damping factor is 0.01 or lower, the damping dissipation is minimal, enabling the energy from the light field to compensate for the dissipation. Thus, the system sustains continuous motion, characterized as a self-vibrating regime. Fig. 3(d) demonstrates this with the presence of a stable limit cycle.

Unedited

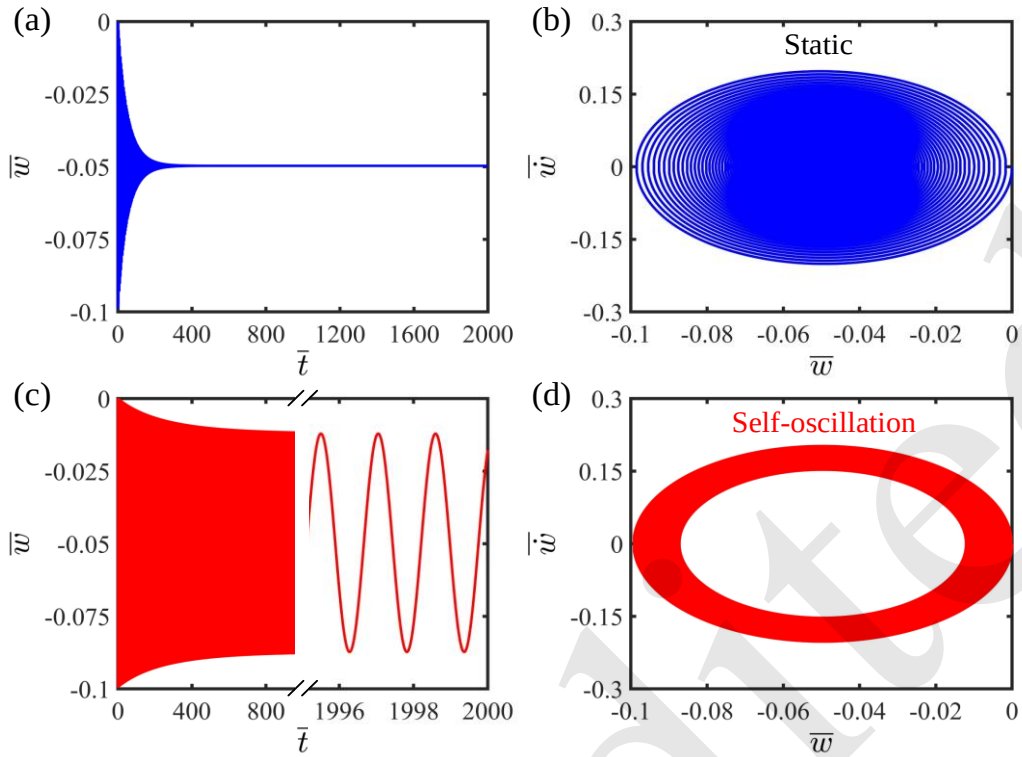

Fig. 3. Two motion regimes of the system. (a) Variation of displacement with time for $\bar{\beta}_1 = 0.05$; (b) Phase diagram for $\bar{\beta}_1 = 0.05$; (c) Variation of displacement with time for $\bar{\beta}_1 = 0.01$; (d) Phase diagram with $\bar{\beta}_1 = 0.01$.

3.2 Solution method

Fig. 4 elucidates the mechanism underlying the self-vibration. The evolution of the tension is depicted in Fig. 4(a), where it displays periodic changes. Fig. 4(b) illustrates the correlation between the tension of the LCE fiber and the end displacement, revealing a hysteresis loop representing the net work done by the tension. Similarly, as shown in Fig. 4(c), the damping force varies periodically with time during the motion. Fig. 4(d) illustrates the dependence of the damping force on the end displacement, where the area of the closed curve represents the damping dissipation. Notably, the net work performed by the tension precisely matches the dissipation energy. Therefore, the heat absorbed by the LCE fiber compensates for the energy expended during self-oscillation, thus enabling self-oscillation to proceed.

Unedited

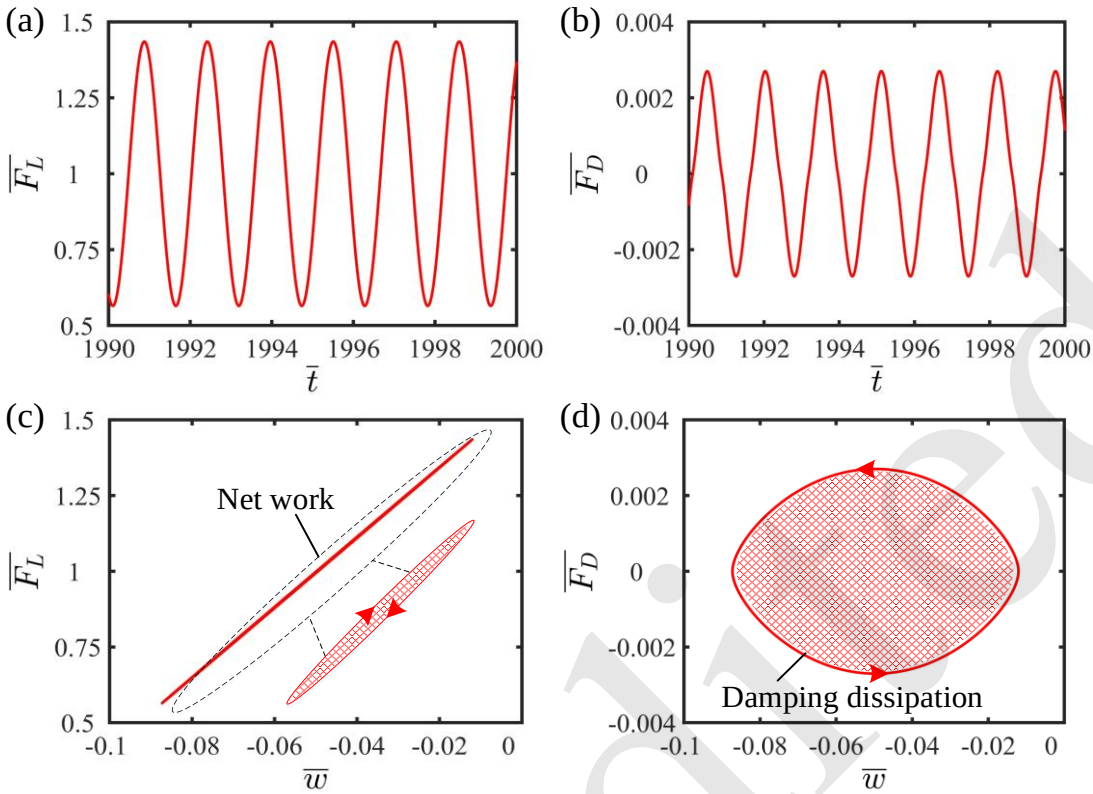

Fig. 4. The mechanism of self-vibration. (a) Time variation of the tension; (b) Time variation of the damping; (c) Plot of the tension versus the end displacement of the LCE fiber; (d) Plot of the damping versus the end displacement of the LCE fiber. The stability of the self-vibration relies on the net work performed by the tension of the LCE fiber.

4 Stability analysis

In this section, we derive analytical solutions for the amplitude and period of the system, and then investigate the system parameters.

4.1 Amplitude and frequency

To facilitate further investigation, we establish the following parameters:

$$\varepsilon_0 = \frac{\overline{K}_{\mathrm{L}}\overline{C}\overline{b}(e^{\overline{C}\overline{b}} - 1 - \overline{C}\overline{b}e^{\overline{C}\overline{b}})}{\left(e^{\overline{C}\overline{b}} - 1\right)^2}\overline{\tau} - \overline{\beta}_1 \qquad (12)$$

$$a_1 = \frac{\overline{\beta}_2\left(1 - e^{\overline{C}\overline{b}}\right)^2}{\overline{\tau}\overline{C}\overline{b}\overline{K}_{\mathrm{L}}(e^{\overline{C}\overline{b}} - \overline{C}\overline{b}e^{\overline{C}\overline{b}} - 1) - \overline{\beta}_1\left(1 - e^{\overline{C}\overline{b}}\right)^2} \qquad (13)$$

$$a_2 = \frac{\overline{K}_{\mathrm{L}}\overline{C}\overline{b}}{e^{\overline{C}\overline{b}} - 1} + \overline{K}_{\mathrm{S}} \qquad (14)$$

$$a_3 = \overline{K}_{\mathrm{L}}\left(\frac{\overline{C}\overline{b}}{e^{\overline{C}\overline{b}} - 1} - 1 - \overline{C}\overline{Q} - \frac{1}{\overline{K}_{\mathrm{L}}}\right) \qquad (15)$$

By substituting the system parameters into Eq. (12), ε_0 can be obtained. For $\varepsilon_0 < 0$, the oscillator cannot oscillate continuously and eventually enters a stationary state. For $\varepsilon_0 > 0$, the system can vibrate continuously and periodically.

From these, Eq. (11) can be re-expressed as:

$$\ddot{\overline{w}} - \varepsilon_0[\dot{\overline{w}} - a_1|\dot{\overline{w}}|\dot{\overline{w}}] + a_2\overline{w} + a_3 = 0 \qquad (16)$$

The amplitude is (Details of the derivation can be found in Section S2 of electronic supplementary materials):

Unedited

$$A=\frac{3\pi}{8\sqrt{\frac{\bar{K}_{\mathrm{L}}\bar{C}\bar{b}}{e^{\bar{C}\bar{b}}-1}+\bar{K}_{\mathrm{S}}}\frac{\bar{\beta}_2\left(1-e^{\bar{C}\bar{b}}\right)^2}{\bar{\tau}\bar{C}\bar{b}\bar{K}_{\mathrm{L}}(e^{\bar{C}\bar{b}}-\bar{C}\bar{b}e^{\bar{C}\bar{b}}-1)-\bar{\beta}_1\left(1-e^{\bar{C}\bar{b}}\right)^2}} \tag{17}$$

and the frequency is:

$$f=\sqrt{\frac{\bar{K}_{\mathrm{L}}\bar{C}\bar{b}}{e^{\bar{C}\bar{b}}-1}+\bar{K}_{\mathrm{S}}} \tag{18}$$

By incorporating specific system parameters, we can ascertain both A and f of the self-vibration. Subsequently, we shall employ the analytical solutions provided by Eqs. (17) and (18) to quantitatively analyze how various parameters affect A and f. We also compare these results with those obtained from numerical calculations.

4.2 Effect of the elastic factor of LCE

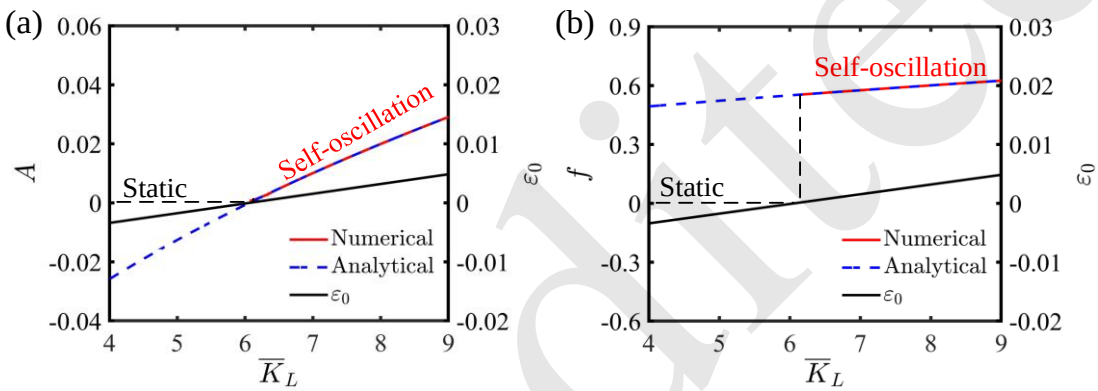

Fig. 5. Effect of $\bar{K}_{\mathrm{L}}$ on the self-vibration. (a) Effect of $\bar{K}_{\mathrm{L}}$ on amplitude and ε_0; (b) Effect of $\bar{K}_{\mathrm{L}}$ on frequency and ε_0

This section investigates the impact of $\bar{K}_{\mathrm{L}}$ on self-vibration. Here, we set the other dimensionless parameters as $\bar{K}_{\mathrm{S}}=5$, $\bar{C}=-0.3$, $\bar{b}=1$, $\bar{\beta}_1=0.01$, $\bar{\beta}_2=0.05$, and $\bar{\tau}=0.01$. Fig. 5 shows that the elastic factor can affect the motion regime of the system. When $\bar{K}_{\mathrm{L}}<6.058$ and $\varepsilon_0<0$, the system is in the static regime, and when $\bar{K}_{\mathrm{L}}>6.058$ and $\varepsilon_0>0$, the system is in the self-vibrational regime. Fig. 5(a) shows that the amplitude exhibits a gradual upward trend with increasing elastic factor. This is because when the elastic factor increases, the photothermally-driven deformation of the LCE fiber is larger, which can increase the amplitude. On the other hand, when the elastic factor decreases, the photothermally-driven deformation is reduced, and so is the amplitude. Fig. 5(b) showcases how $\bar{K}_{\mathrm{L}}$ can enhance *f*, which is an intuitive result. When the elastic factor rises, the driving force increases, which increases the oscillation rate of the system. It is also apparent in Fig. 5 that the numerical results are quite close to the analytical solutions.

4.3 Effect of the elastic factor of the spring

Unedited

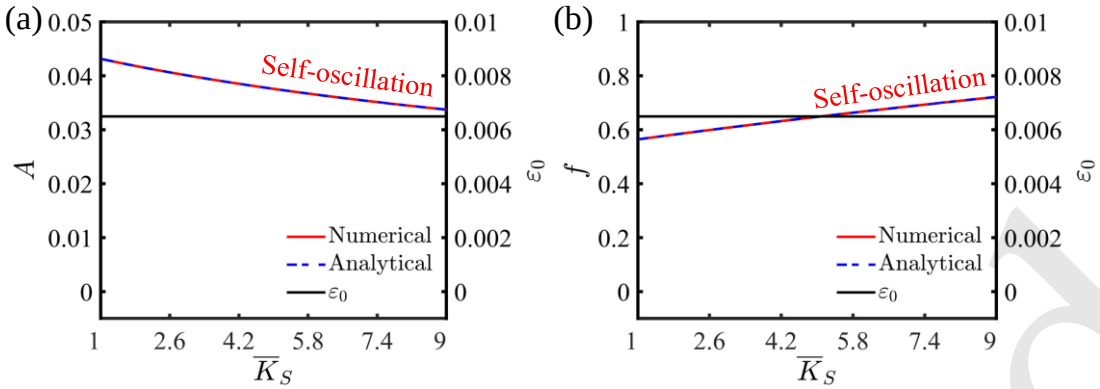

Fig. 6. Effect of $\overline{K}_S$ on the self-vibration. (a) Effect of $\overline{K}_S$ on amplitude and ε_0; (b) Effect of $\overline{K}_S$ on frequency and ε_0.

Fig. 6 shows the effect of $\overline{K}_S$ on the self-vibration, when $\overline{K}_L = 10$, $\overline{C} = -0.3$, $\overline{b} = 1$, $\overline{\beta}_1 = 0.01$, $\overline{\beta}_2 = 0.05$, and $\overline{\tau} = 0.01$. It's possible to show that no matter how the elastic factor of the spring is adjusted, the system can always self-vibrate. This is because the motion regime is determined by ε_0, which is not dependent on $\overline{K}_S$, and thus changing $\overline{K}_S$ does not affect the motion regime. Fig. 6 suggests that the amplitude decreases with the increasing elastic factor of the spring, while the frequency increases. This result is consistent with a classical vibrating spring system. Boosting the elastic factor of the spring translates to a heightened restoring force, which in turn quells the system's oscillation, as shown in Fig. 6(a). In contrast, when the elastic factor decreases, the restoring force decreases, and then the amplitude increases. When the amplitude decreases, the oscillation distance decreases, and the corresponding time also decreases, thus increasing the frequency, as depicted in Fig. 6(b). Fig. 6 demonstrates that when the system is in the self-vibrating regime, the numerical results match those derived from the analytical solutions.

4.4 Effect of the thermal contraction factor

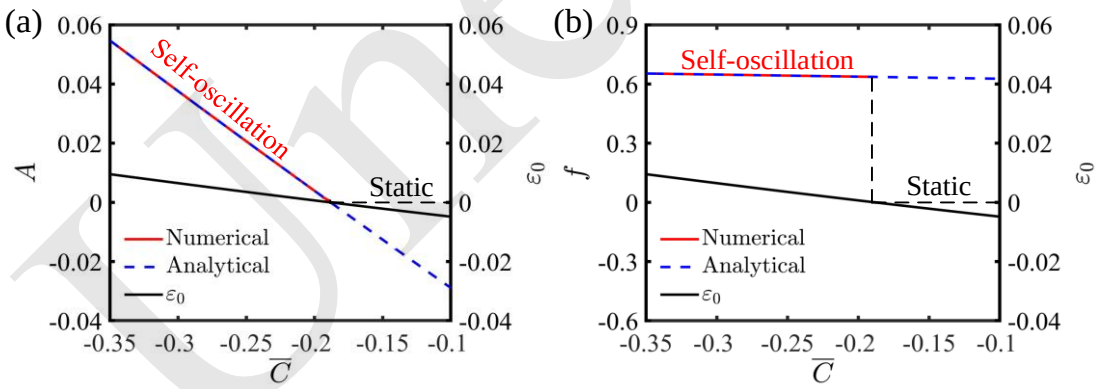

Fig. 7. Effect of $\overline{C}$ on the self-vibration. (a) Effect of $\overline{C}$ on amplitude and ε_0; (b) Effect of $\overline{C}$ on frequency and ε_0.

Fig. 7 presents the effect of $\overline{C}$ on the self-vibration, when $\overline{K}_L = 10$, $\overline{K}_S = 5$, $\overline{b} = 1$, $\overline{\beta}_1 = 0.01$, $\overline{\beta}_2 = 0.05$, and $\overline{\tau} = 0.01$. We can see how the thermal contraction factor significantly influences the system's motion regime. The critical value that bifurcates the two motion regimes is shown as $\overline{C} = -0.1833$. When this critical value is exceeded, ε_0 is less than zero according to the Hurwitz criterion, and the system evolves into a stationary state. Conversely, ε_0 is greater than zero when the thermal contraction factor is lower than the critical value, the system is in a self-vibrating regime. Fig. 7(a) shows how the amplitude decreases with increasing $\overline{C}$. When the thermal contraction factor is small, the fiber

Unedited

can harvest the light energy more efficiently, thus enlarging the amplitude. Conversely, when the thermal contraction factor is large, the absorption of light energy is less efficient, which results in a smaller amplitude. As one can observe in Fig. 7(b), as the thermal contraction factor increases, the self-vibration frequency declines. The plots in Fig. 7 further demonstrate the similarity between the numerical results from the Runge-Kutta method and those derived from analytical solutions. When the system is in the static regime (that is, $\varepsilon_0 < 0$), the results of the numerical and analytical calculations no longer align.

4.5 Effect of the gradient of heat flux

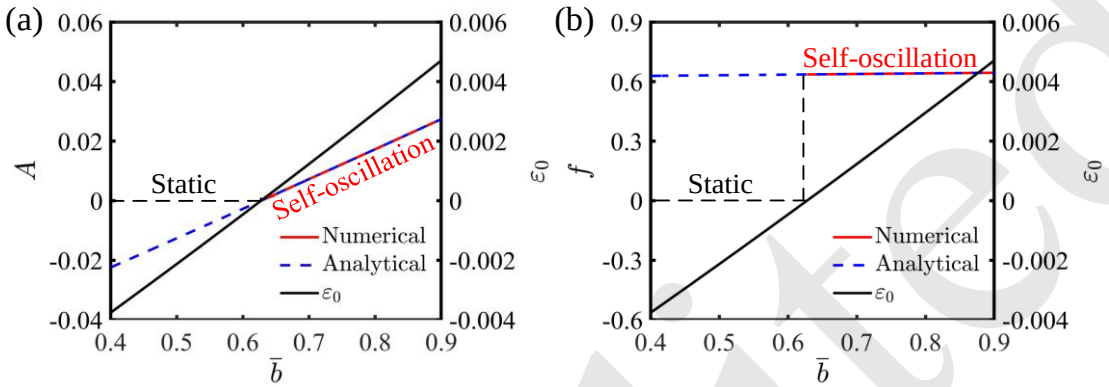

Fig. 8. Effect of $\bar{b}$ on the self-vibration. (a) Effect of $\bar{b}$ on amplitude and ε_0; (b) Effect of $\bar{b}$ on frequency and ε_0.

Fig. 8 demonstrates how $\bar{b}$ affects the self-vibration, when $\bar{K}_L = 10$, $\bar{K}_S = 5$, $\bar{C} = -0.3$, $\bar{\beta}_1 = 0.01$, $\bar{\beta}_2 = 0.05$, and $\bar{\tau} = 0.01$. $\bar{b}$ effectively determines the motion regime of the system, where $\bar{b} < 0.627$ and $\varepsilon_0 < 0$ corresponds to the static regime, $\bar{b} > 0.627$ and $\varepsilon_0 > 0$ corresponds to the self-vibrating regime. This can be understood by considering the case of constant-gradient light, where the LCE fiber continuously contracts until it reaches maximum strain and then enters a static regime. Fig. 8(a) shows how the heat flux affects the amplitude of self-oscillation, where the larger $\bar{b}$ is, the greater the amplitude of self-oscillation. This aligns with physical intuition and mirrors observations in other self-oscillating systems, where increased light intensity resulted in a higher amplitude of self-oscillation (Zeng et al., 2016). The underlying reason for this phenomenon is that a larger gradient of heat flux drives the system to absorb more light energy, which enhances the amplitude. Fig. 8(b) shows that the frequency essentially remains constant as the gradient of heat flux changes. Essentially, the self-vibration frequency is determined by its natural frequency, and a change in the gradient of heat flux cannot influence the natural frequency. Again, a comparison between the numerical and analytical calculations shows that the amplitudes and frequencies are almost the same in the self-vibrating regime. On the other hand, the results obtained by the two methods diverge when the system is in the static regime, with $\varepsilon_0 < 0$.

4.6 Effect of the first damping factor

Unedited

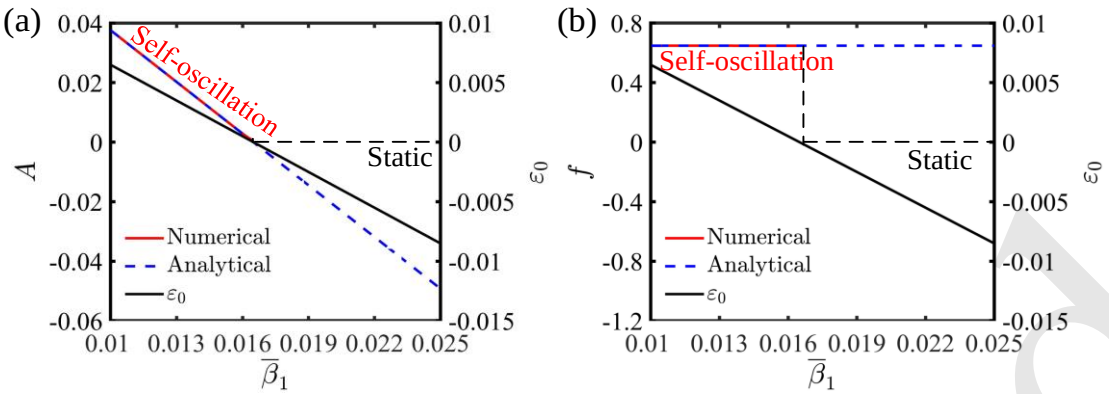

Fig. 9. Effect of $\bar{\beta}_1$ on the self-vibration. (a) Effect of $\bar{\beta}_1$ on amplitude and ε_0; (b) Effect of $\bar{\beta}_1$ on frequency and ε_0.

This section delves into the impact of $\bar{\beta}_1$ on self-vibration, when $\bar{K}_L = 10$, $\bar{K}_S = 5$, $\bar{C} = -0.3$, $\bar{b} = 1$, $\bar{\beta}_2 = 0.05$, and $\bar{\tau} = 0.01$. Fig. 9 shows that the motion regime of the system is significantly influenced by the first damping factor. The critical value of this first damping factor, required to switch between the self-vibrating and static regimes, is $\bar{\beta}_1 = 0.0165$. This is because the critical value is related to the Hurwitz criterion: when $\bar{\beta}_1 < 0.0165$ and $\varepsilon_0 < 0$, the system is asymptotically stable (i.e. in the static regime), and when $\bar{\beta}_1 > 0.0165$ and $\varepsilon_0 > 0$, the system evolves into the self-vibrating regime. From Fig. 9(a), it is evident that $\bar{\beta}_1$ can inhibit self-vibration, with a larger factor value corresponding to smaller amplitudes. Energy compensation explains this phenomenon. With a larger $\bar{\beta}_1$, the damping dissipation increases, resulting in a reduction in the system's kinetic energy and a decrease in amplitude. Conversely, a smaller first damping factor reduces the damping dissipation, allowing more light energy to be converted into kinetic energy, and leading to a larger amplitude. Fig. 9(b) indicates that $\bar{\beta}_1$ does not significantly impact the frequency. Again, we can see that the numerically-calculated results match the analytical solutions.

4.7 Effect of the second damping factor

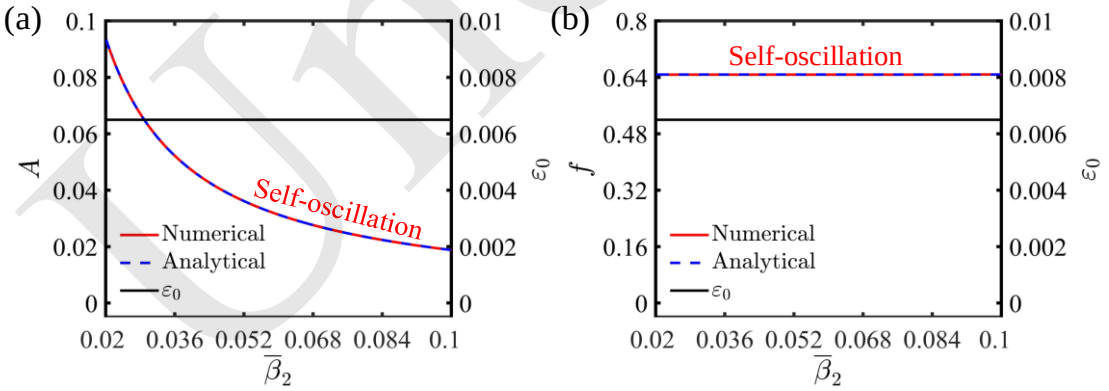

Fig. 10. Effect of $\bar{\beta}_2$ on the self-vibration. (a) Effect of $\bar{\beta}_2$ on amplitude and ε_0; (b) Effect of $\bar{\beta}_2$ on frequency and ε_0.

This section investigates how $\bar{\beta}_2$ affects the self-vibration, when $\bar{K}_L = 10$, $\bar{K}_S = 5$, $\bar{C} = -0.3$, $\bar{b} = 1$, $\bar{\beta}_1 = 0.01$, and $\bar{\tau} = 0.01$. Fig. 10 shows how the motion regime remains unaffected by the second damping factor. The reason for this is similar to the case of the spring's elastic factor. According to the Hurwitz criterion, the motion regime is determined by ε_0, which is not dependent on $\bar{\beta}_2$, and thus the changing of $\bar{\beta}_2$ does not affect the motion regime. It is evident from Fig. 10(a) that as the second damping factor increases, the amplitude gradually declines,

Unedited

while the frequency remains the same. This is because a smaller $\bar{\beta}_2$ reduces the system's damping dissipation, and thus more light energy is converted into kinetic energy, leading to a larger amplitude. On the other hand, a larger second damping factor increases the system's damping dissipation, and the kinetic energy converted from light energy is reduced, consequently reducing the amplitude. As shown in the plots in Fig. 10, the numerical results closely match the analytical solutions.

4.8 Effect of the characteristic time

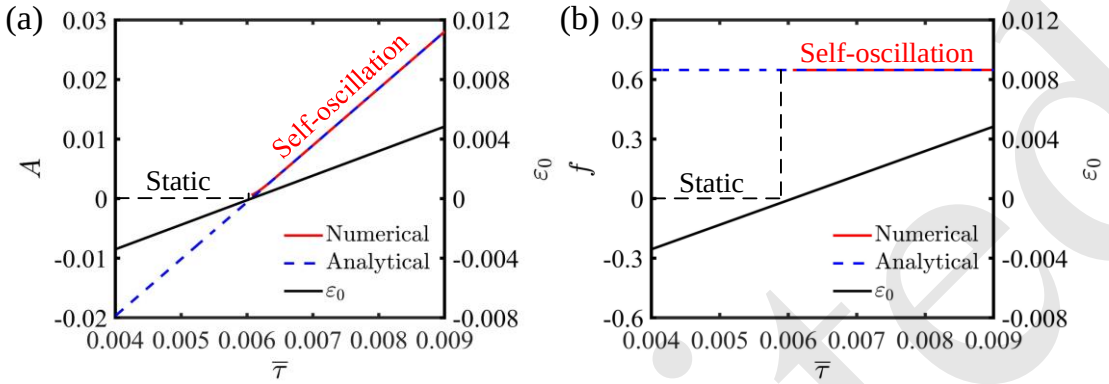

Fig. 11. Effect of $\bar{\tau}$ on the self-vibration. (a) Effect of $\bar{\tau}$ on amplitude and ε_0; (b) Effect of $\bar{\tau}$ on frequency and ε_0.

In this section, we delve into how $\bar{\tau}$ influences self-vibration, when $\bar{K}_L = 10$, $\bar{K}_S = 5$, $\bar{C} = -0.3$, $\bar{b} = 1$, $\bar{\beta}_1 = 0.01$, and $\bar{\beta}_2 = 0.05$. As illustrated in Fig. 11, the critical characteristic time $\bar{\tau} = 0.0061$is the value at which the self-vibrating regime is entered. When $\bar{\tau} < 0.0061$ and $\varepsilon_0 < 0$, the system is in the static regime, and when $\bar{\tau} > 0.0061$ and $\varepsilon_0 > 0$, the system is in the self-vibrating regime. Fig. 11(a) depicts how the amplitude increases as the characteristic time grows. This is because as $\bar{\tau}$ increases, the LCE fiber absorbs more light energy, facilitating greater conversion into kinetic energy and larger amplitude. Fig. 11(b) shows that the effect of the characteristic time on the frequency is almost negligible. Additionally, we can see that the numerical outcomes from the Runge-Kutta method closely resemble the analytical results from the multi-scale method in the self-vibrating regime. However, a discrepancy arises between the numerical and analytical results when the system enters the static regime, with $\varepsilon_0 < 0$.

5 Conclusions

Current research on self-vibrating systems tends to focus on determining the amplitude, frequency, equilibrium position, bifurcation points, and other characteristics. The conventional approach to solving for these characteristics is using numerical methods, however, such methods suffer from limitations such as high computational complexity, which have impeded advancements in the design and utilization of self-vibrating systems. Thus in this study, we aimed to analytically describe an LCE fiber-spring system, which generates periodic oscillations when exposed to spatially-constant gradient light. Utilizing a dynamic model for LCE, we derived and linearized control equations for the self-vibrating LCE fiber-spring system. Two modes of motion, the static regime and the self-vibrating regime, were revealed with numerical methods, along with the mechanism of energy compensation. Next, we analyzed the system using the Hurwitz criterion, and an analytical method was utilized to determine the frequency and amplitude.

The results demonstrate that the elastic factor, the thermal contraction factor of LCE, the gradient of heat flux, and the characteristic time can all promote the amplitude, while the elastic factor of the spring, the first damping factor, and the second damping factor can all inhibit the vibration. The elastic factor of LCE, the thermal contraction factor of LCE, and the elastic factor of the spring can increase the system's vibrational frequency. Furthermore, we demonstrated that the amplitudes and frequencies calculated by the Runge-Kutta numerical method and the multi-scale analytical method are consistent. Overall, the multi-scale method enables accurate mathematical description and analysis of

Unedited

self-vibrating systems, particularly those with stimulus-responsive active materials.

Acknowledgments

This study is supported by National Natural Science Foundation of China (No. 12172001), University Natural Science Research Project of Anhui Province (No. 2022AH020029), Anhui Provincial Natural Science Foundation (Nos. 2208085Y01 and 2008085QA23) and Housing and Urban-Rural Development Science and Technology Project of Anhui Province (No. 2023-YF129).

Author contributions

Kai LI designed the research. Haiyang WU and Jiangfeng LOU processed the corresponding data. Haiyang WU and Biao ZHANG wrote the first draft of the manuscript. Yuntong DAI helped to organize the manuscript. Kai LI and Haiyang WU revised and edited the final version.

Conflict of interest

Haiyang WU, Jiangfeng LOU, Yuntong DAI, Biao ZHANG, Kai LI declare that they have no conflict of interest.

References

Li MH, Keller P, Li, B, et al., 2003. Light-driven side-on nematic elastomer actuators. *Advanced Materials*,15:569–572. https://doi.org/10.1002/adma.200304552

Wang X, Tan CF, Chan KH, et al., 2018. In-built thermo-mechanical cooperative feedback mechanism for self-propelled multimodal locomotion and electricity generation. *Nature Communications*, 9:3438. https://doi.org/10.1038/s41467-018-06011-9

Nocentini S, Parmeggiani C, Martella, D, et al., 2018. Optically driven soft micro robotics. *Advanced Optical Materials*, 6:1800207. https://doi.org/10.1002/adom.201800207

Ge F, Yang R, Tong X, et al., 2018. A multifunctional dyedoped liquid crystal polymer actuator: light-guided transportation, turning in locomotion, and autonomous motion. *Angewandte. Chemie-International Edition*, 57:11758–11763. https://doi.org/10.1002/ange.201807495

Preston DJ, Jiang HJ, Sanchez V, et al., 2019. A soft ring oscillator. *Science Robotics*, 4:5496.. https://doi.org/10.1126/scirobotics.aaw5496

Zeng H, Lahikainen, M, Liu L, et al., 2019. Light-fuelled freestyle self-oscillators. *Nature Communications*,10:1-9. https://doi.org/10.1038/s41467-019-13077-6

Ding W, 2010. Self-excited vibration. Springer Berlin/Heidelberg, Germany .

Baumann A, Sánchez-Ferrer A, Jacomine L, et al., 2018. Motorizing fibres with geometric zero-energy modes. *Nature Materials*, 17:523–527. https://doi.org/10.1038/s41563-018-0062-0

Kageyama Y, Ikegami T, Satonaga S, et al., 2020. Light-driven flipping of azobenzene assemblies-sparse crystal structures and responsive behavior to polarized light. *Chemistry-a European Journal*, 26:10759–10768. https://doi.org/10.26434/chemrxiv.11786088.v1

Liao B, Zang H, Chen M, et al., 2008. Soft rod-climbing robot inspired by winding locomotion of snake. *Soft Matter*, 4:1796–1798. https://doi.org/10.1089/soro.2019.0070

White TJ, Tabiryan NV, Serak SV, et al., A high frequency photodriven polymer oscillator. Soft Matter **4**, 1796–1798 (2008).

Fang P Dai LM, Hou YJ, et al., 2019. The study of identification method for dynamic behavior of high-dimensional nonlinear system. *Shock and Vibration*,3497410. https://doi.org/10.1155/2019/3497410

Thomson WT, 2005. Theory of vibration with applications, 5th ed. Prentice-Hall: Hoboken, NJ, USA.

Pivnenko M, Fedoryako A, Kutulya, L, et al., 1999. Resonance phenomena in a ferroelectric liquid crystal near the phase transition SmA-SmC*. *Molecular Cryltals Liquid Crystals*, 328:111-118. https://doi.org/10.1080/10587259908026051

Wu H, Zhang B, Li K, 2024. Synchronous behaviors of three coupled liquid crystal elastomer-based spring oscillators under linear temperature fields. *Physical Review E*, 109:024701. https://doi.org/10.1103/PhysRevE.109.024701

Xu P, Sun X, Dai Y, et al., 2024. Light-powered sustained chaotic jumping of a liquid crystal elastomer balloon. *International Journal of Mechanical Science*, 266:108922. https://doi.org/10.1016/j.ijmecsci.2023.108922

Kumar, K., Knie, C., Bléger, D., et al., 2016. A chaotic self-oscillating sunlight-driven polymer actuator. *Nature. Communications*, 7:11975. https://doi.org/10.1038/ncomms11975

Xu P, Chen Y, Wu H, et al., 2024. Chaotic motion behaviors of liquid crystal elastomer pendulum under periodic illumination. *Results in Physics*, 10:7332. https://doi.org/10.1016/j.rinp.2024.107332

Shastri A, McGregor L, Liu Y, et al., 2015. An aptamer-functionalized chemomechanically modulated biomolecule catch-and-release system. *Nature Chemistry*, **7:**447-454. https://doi.org/10.1038/nchem.2203

He Q, Yin R, Hua Y, et al., 2023. A modular strategy for distributed, embodied control of electronics-free soft robots. *Science Advanced*, 9:eade9247. https://doi.org/10.1126/sciadv.ade9247

Wang Y, Yin R, Jin L, et al., 2023. 3D-printed photoresponsive liquid crystal elastomer composites for free-form actuation. *Advanced Functional Materials*, 33:2210614. https://doi.org/10.1002/adfm.202210614

Yu Y, Hu H, Dai Y, et al., 2024. Modeling the light-powered self-rotation of a liquid crystal elastomer fiber-based engine. *Physical Review E*, 109:034701. https://doi.org/10.1103/PhysRevE.109.034701

Unedited

Sun J, Wang Y, Liao W, et al., 2021. Ultrafast, High-Contractile Electrothermal-Driven Liquid Crystal Elastomer Fibers towards Artificial Muscles. *Small*, **17**(44):2103700. https://doi.org/10.1002/smll.202103700

Boissonade J, and Kepper PD, 2011. Multiple types of spatio-temporal oscillations induced by differential diffusion in the Landolt reaction. *Physical Chemistry Chemical Physics*, **13**:4132–4137. https://doi.org/10.1039/C0CP01653E

Hua M, Kim C, Du Y, et al., 2021. Swaying gel: Chemo-mechanical self-oscillation based on dynamic buckling. *Matter* 4:1029-1041. https://doi.org/10.1016/j.matt.2021.01.002

Yoshida R, 2010. Self-oscillating gels driven by the Belousov-Zhabotinsky reaction as novel smart materials. *Advanced. Materials*, 22, 3463–3483. https://doi.org/10.1002/adma.200904075

Wang Y, Liu J, Yang S, 2022. Multi-functional liquid crystal elastomer composites. *Applied Physics Reviews*, 9:011301. https://doi.org/10.1063/5.0075471

Wang Y, and Xiao J, 2021. Confined thin film wrinkling on shape memory polymer with hybrid surface morphologies. *Acta Mechanica Sinica*, 37:1063–1071. https://doi.org/10.1007/s10409-021-01106-x

Chen G, Xian W, Wang Q, et al., 2021. Molecular simulation-guided and physics-informed mechanistic modeling of multifunctional polymers. *Acta Mechanica Sinica*, **37**:725–745. https://doi.org/10.1007/s10409-021-01100-3

Hu Y, Ji Q, Huang M, et al., 2021. Light-driven self-oscillating actuators with phototactic locomotion based on black phosphorus heterostructure. *Angewandte. Chemie-International Edition*, 60:20511–20517. https://doi.org/10.1002/ange.202108058

Wang L, Wei Z, Xu Z, et al., 2023. Shape morphing of 3D printed Liquid crystal elastomer structures with precuts. *ACS Applied Polymer Materials*,**5**(9):7477-7484. https://doi.org/10.1021/acsapm.3c01335

Dai L, Wang L, Chen B, et al., 2023. Shape memory behaviors of 3D printed liquid crystal elastomers. *Soft Science*, 3(1):4. https://doi.org/10.20517/ss.2022.28

Yang H, Zhang C, Chen B, et al., 2023. Bioinspired design of stimuli-responsive artificial muscles with multiple actuation modes. *Smart Materials and Structures*, 32(8):085023. https://doi.org/10.1088/1361-665X/ace4a9

Chen B, Liu C, Xu Z, et al., 2024. Modeling the thermo-responsive behaviors of polydomain and monodomain nematic liquid crystal elastomers. *Mechanics of Materials*, 188:104838. https://doi.org/10.1016/j.mechmat.2023.104838

Bai C, Kang J, Wang Y, 2024. Light-induced motion of three-dimensional pendulum with liquid crystal elastomeric fiber. *International Journal of Mechanical Science*, 266:108911 .

Wang Y, Dang A, Zhang Z, et al., 2020. Repeatable and reprogrammable shape morphing from photoresponsive gold nanorod/liquid crystal elastomers. *Advanced. Materials*, **32**:2004270 . https://doi.org/10.1016/j.ijmecsci.2023.108911

Guo YL, Liu N, Cao Q, et al., 2022. Photothermal diol for NIR-responsive liquid crystal elastomers. *Acs Applied Polymer Materials*, **4**:6202-6210 . https://doi.org/10.1021/acsapm.2c00969

Cui Y, Yin YF, Wang CJ, et al., 2019. Transient thermo-mechanical analysis for bimorph soft robot based on thermally responsive liquid crystal elastomers. *Applied Mathematics and Mechannics-English*, 40:943-952 . https://doi.org/10.1007/s10483-019-2495-8

Liao W, and Yang Z, 2022. The integration of sensing and actuating based on a simple design fiber actuator towards intelligent soft robots. *Advanced Materials Technologies*, 7(6):2101260. https://doi.org/10.1002/admt.202101260

Haber JM, Sanchez-Ferrer A, Mihut AM, 2013. Liquid-crystalline elastomer-nanoparticle hybrids with reversible switch of magnetic memory. *Advanced Materials*, 25:1787-1791.

Wang Y, Yin R, Jin L, et al., 2022. 3D-Printed photoresponsive liquid crystal elastomer composites for free-form actuation. *Advanced Functional Materials*, 2210614. https://doi.org/10.1002/adfm.202210614

Harris KD, Bastiaansen C, Lub J, et al., 2005. Self-assembled polymer films for controlled agent-driven motion. *Nano Letters*. 9:1857-1860. https://doi.org/10.1021/nl0514590

Wu H, Lou J, Zhang B, et al., 2024. Stability analysis of a liquid crystal elastomer self-oscillator under a linear temperature field. *Applied Mathematics and Mechanics*, 45(2):337-354. https://doi.org/10.1007/s10483-024-3080-5

Wu H, Dai Y, Li K, 2023. Self-vibration of liquid crystal elastomer strings under steady illumination. *Polymers*, 15:3483. https://doi.org/10.3390/polym15163483

Liu J, Shi Feng, Song W, et al., 2024. Modeling of self-oscillating flexible circuits based on liquid crystal elastomers. *International Journal of Mechanical Science*, 270:109099. https://doi.org/10.1016/j.ijmecsci.2024.109099

Zuo W, Sun T, Dai Y, et al., 2023. Light-powered self-propelled trolley with a liquid crystal elastomer pendulum motor. *International Journal of Solids and Structures*, 285:112500. https://doi.org/10.1016/j.ijsolstr.2023.112500

Xu P, Chen Y, Sun X, et al., 2024. Light-powered self-sustained chaotic motion of a liquid crystal elastomer-based pendulum. Chaos Soliton and Fractals, 184:115027. https://doi.org/10.1016/j.chaos.2024.115027

Yu Y, Hu H, Wu H, et al., 2024. A light-powered self-rotating liquid crystal elastomer drill. *Heliyon* 10(5):e27748. https://doi.org/10.1016/j.heliyon.2024.e27748

Ge D, Dai YT, Li K, 2023. Self-Sustained euler buckling of an optically responsive rod with different boundary constraints. *polymers* 15:316 . https://doi.org/10.3390/polym15020316

Unedited

Manna RK, Shklyaev OE, Balazs AC, 2021. Chemical pumps and flflexible sheets spontaneously form self-regulating oscillators in solution. *Proceedings of the National Academy of Sciences of the United States of America* 118:e2022987118 . https://doi.org/10.1073/pnas.2022987118

Li Z, Myung NV, Yin Y, et al., 2021. Light-powered soft steam engines for self-adaptive oscillation and biomimetic swimming. *Science Robotics*, 6:eabi4523. https://doi.org/10.3390/polym15020344

Bazir A, Baumann A, Ziebert F, et al., 2020. Dynamics of fiberboids. *Soft Matter* 16:5210–5223. https://doi.org/10.1039/D0SM00540A

Zhou L, Chen H, Li K, 2024. Optically-responsive liquid crystal elastomer thin film motors in linear/nonlinear optical fields. *Thin Wall Structures*, 202:112082. https://doi.org/10.1016/j.tws.2024.112082

Yu Y, Du CS, Li K, et al., 2022. Controllable and versatile self-motivated motion of a fiber on a hot surface. *Extreme Mechanics Letters*, 57:101918 . https://doi.org/10.1016/j.eml.2022.101918

Kim Y, Berg J, Crosby AJ, 2021. Autonomous snapping and jumping polymer gels. *Nature Materials*, 20:1695–1701. https://doi.org/10.1038/s41563-020-00909-w

Yu Y, Zhou L, Du C, et al., 2024. Self-galloping of a liquid crystal elastomer catenary cable under a steady temperature field. *Thin Wall Structures*, 202:112071. https://doi.org/10.1016/j.tws.2024.112071

Cheng QB, Cheng WY, Dai YT, et al., 2023. Self-oscillating floating of a spherical liquid crystal elastomer balloon under steady illumination. *International Journal of Mechanical Science*,241:107985. https://doi.org/10.1016/j.ijmecsci.2022.107985

Serak S, Tabiryan NV, Vergara R, et al., 2010. Liquid crystalline polymer cantilever oscillators fueled by light. *Soft Matter*, 6:779–783. https://doi.org/10.1039/B916831A

Chakrabarti A, Choi GPT, Mahadevan L, 2020. Self-excited motions of volatile drops on swellable sheets. *Physical Review Letters*, 124:258002. https://doi.org/10.1103/PhysRevLett.124.258002

Fu L, Zhao W, Ma J, et al., 2022. A humidity-powered soft robot with fast rolling locomotion.*Research*,9832901. https://doi.org/10.34133/2022/9832901

Cheng Y, Lu H, Lee X, et al., 2019. Kirigami-based light-induced shapemorphing and locomotion. *Advanced Materials*,32:1906233. https://doi.org/10.1002/adma.201906233

McLachlan RI, Sun Y, Tse PSP, 2011. Linear stability of partitioned Runge-kutta methods. *Siam Journal on Numerical. Analysis*, 49:232-263. https://doi.org/10.1137/100787234

März R, 1984. On Difference and Shooting Methods for Boundary Value Problems in Differential-Algebraic Equations. *ZAMM-Journal of Applied Mathematics and Mechanics/Zeitschrift für Angewandte Mathematik und Mechanik*, **64**(11):463-473 (1984). https://doi.org/10.1002/zamm.19840641108

Patidar K, 2005. On the use of nonstandard finite difference methods. *Journal of Differential equations*,11(8):735-758. https://doi.org/10.1080/10236190500127471

Allgower E, and Georg K, 2012. Numerical continuation methods: an introduction. *Springer*, 13.

Fan S, and Shen Y, 2022. Extension of multi-scale method and its application to nonlinear viscoelastic system. *Chinese Journal of Theoretical and Applied Mechanics*, 54:495-502. https://doi.org/10.6052/0459-1879-21-487

Li J, Zhang J, Zhang W, et al., 2004. Multi-scale methodology for complex systems. Chemical. Engineering Science,59:1687-1700. https://doi.org/10.1016/j.ces.2004.01.025

Liu W, Hao S, Belytschko T, Li S, et al. 2000. Multi-scale methods. International Journal for Numerical Methods in Engineering, 47(7), 1343-1361. https://doi.org/10.1002/(SICI)1097-0207(20000310)47:7<1343::AID-NME828>3.0.CO;2-W

Wen B, Li Y, Han Q, 2007. Analytical methods and engineering applications in nonlinear vibration theory. *Northeastern University Press*.

Panton R, 2013. Asymptotic analysis methods. *Incompressible Flow*, 374-408. https://doi.org/10.1002/9781118713075.ch15

Cheung YK, Chen SH, Lau SL, 1990. Application of the incremental harmonic balance method to cubic non-linearity systems. *Journal of Sound and Vibration*, 140:273-286. https://doi.org/10.1016/0022-460X(90)90528-8

Yan Z, Dai H, Wang Q, et al., 2023. Harmonic balance methods: a review and recent developments. *Cmes-Computer Modeling in Engineering and science*, 1-41. https://doi.org/10.32604/cmes.2023.028198

Vestroni F, Luongo A, Paolone A, 2008. A perturbation method for evaluating nonlinear normal modes of a piecewise linear two-degrees-of-freedom system. *Nonlinear Dynamics*, 54:379-393. https://doi.org/10.1007/s11071-008-9337-3

Nayfeh AH, 1965. A perturbation method for treating nonlinear oscillation problems. *Studies in Applied Mathematics*, 44:368-374. https://doi.org/10.1002/sapm1965441368

Nayfeh AH, and Mook DT, 1979. Nonlinear Oscillations. *John Wiley & Sons*.

Nayfeh AH, 1993. Introduction to Perturbation Techniques. *John Wiley & Sons*.

Nayfeh AH and Pai PF, 2008. Linear and nonlinear structural mechanics. *John Wiley & Sons*. https://doi.org/10.1002/9783527617562

Sturrock PA and surName G,1957. Non-linear effects in electron plasmas. *Proceedings Of The Royal Society A-mathematical Physical And Engineering Sciences*, 242(1230):277-299.

He Q, Wang Z, Wang Y, et al., 2021. Electrospun liquid crystal elastomer microfiber actuator. *Science Robotics*, 6:eabi9704. https://doi.org/10.1126/scirobotics.abi9704

Unedited

Heller MD, 2005. Hurwitz-based stability criteria for bounded nonlinear time-varying systems. *International Congress & Convention Association*,1:942-947. https://doi.org/10.1109/ICCA.2005.1528257.

Ho MT, Datta A, Bhattacharyya S, 1998. An elementary derivation of the Routh-Hurwitz criterion. *IEEE Transactions on Automatic control*,43(3):405-409. https://doi.org/10.1109/9.661607.

Nagele T, Hoche R, Zinth W, et al., 1997. Femtosecond photoisomerization of cis-azobenzene. *Chemical Physics Letters*, 272:489-495. https://doi.org/10.1016/S0009-2614(97)00531-9

Electronic supplementary materials

Sections S1 and S2

中文概要

题　目:恒定梯度光下液晶弹性体纤维-弹簧自振系统的多尺度分析

作　者: 吴海洋，娄江风，戴云彤，张彪，李凯

机　构: 安徽建筑大学大学，土木工程学院，中国合肥，230601

目　的: 目前基于主动材料的自振动系统的解析解的难以获得，阻碍了该类自振动系统的设计与应用。我们的目标是加深对液晶弹性体纤维弹簧系统的理解，得到液晶弹性体纤维弹簧系统的自振动解析解和稳定性判据。

创新点: 1. 推导出液晶弹性体纤维-弹簧自振动系统稳定性判据；2. 推导出液晶弹性体纤维-弹簧自振动系统的幅度和频率解析解。

方　法: 1. 提出了一种空间线性光场下的液晶弹性体纤维-弹簧自振动系统；2. 通过数值计算确定的两种不同的运动模式，阐明了自振动的机制；3. 将控制方程线性化处理并使用 Hurwitz 准则进行分岔分析；4. 使用多尺度方法对控制方程进行分析，确定振幅和周期的解析解。

结　论: 1. 系统的自振动模式和振幅及频率可由系统参数调节；2. 运用多尺度方法对液晶弹性体纤维-弹簧自振动系统进行分析求解，得到的振幅和频率结果与数值结果一致，计算效率大幅提升。

关键词: 自振动；恒定梯度光；液晶弹性体；多尺度法

Unedited